Ultrafast Electron Dynamics at Metal Interfaces: Intraband Relaxation of Image State Electrons as Friction

Sean Garrett-Roe, Steven T. Shipman, Paul Szymanski,† Matthew L. Strader, Aram Yang, and Charles B. Harris*

Chemistry Department, U.C. Berkeley, Berkeley, California 94720, and Chemical Sciences Division, E.O. Lawrence Berkeley National Lab, Berkeley, California 94720

Received: April 16, 2005; In Final Form: June 24, 2005

Two-photon photoemission of image potential states above monolayers of *p*-xylene/Ag(111) shows that electrons with different momenta have very different rise and decay rates as a function of parallel momentum. The dynamics are due to energy and momentum loss (intraband relaxation), which we model as a stochastic process isomorphic to the overdamped motion of a harmonic oscillator. The method extracts a friction coefficient from the data which can be explained by electron−electron scattering in a formalism based on the Lindhard dielectric function. One-electron excitations (interband transistions) dominate the dissipation mechanism, with a smaller contribution from collective electronic excitations (plasmons).

1. Introduction

Studying the dynamics of an excess electron at a metal interface has both practical and theoretical importance. The practical uses include organic light emitting diodes (OLEDs) and molecular electronics, while the theoretical issues touch on electron solvation and localization in systems with reduced dimensionality. These dynamics occur on the femtosecond to picosecond time scale and involve changes in electron energies, momenta, and even spatial extent, all of which can be measured with time- and angle-resolved two-photon photoemission (2PPE).[1−3]

In a 2PPE experiment, an ultrafast laser excites an electron from below the Fermi level of the metal substrate into an initially unoccupied state; after a delay time, τ, a probe photon photoemits the electron, sending it to a detector (Figure 1a). From the kinetic energy of the electron, one can deduce the binding energy of the intermediate electronic state. For this discussion, the relevant electronic states are image potential states (IPS). An electron outside a metal surface induces a surface charge on the metal, which can be represented as an image charge[4] (Figure 1c). The electron is bound to the surface by the Coulomb attraction to this image charge, which leads to a quantized series of states labeled by their principle quantum number, n (Figure 1d). The electrons occupying these IPS are bound in the direction normal to the surface, but are initially free-electron-like in the parallel directions. The angle between the metal substrate and the detector is an experimental variable that allows one to detect electrons with a specific amount of momentum parallel to the surface. That is, as the surface normal is rotated from the detector, only electrons with a particular amount of parallel momentum will reach the detector (Figure 1b). Several reports have observed that IPS electrons with different momenta have different lifetimes and that electrons accumulate at low momenta.[5,6] These observations are consistent

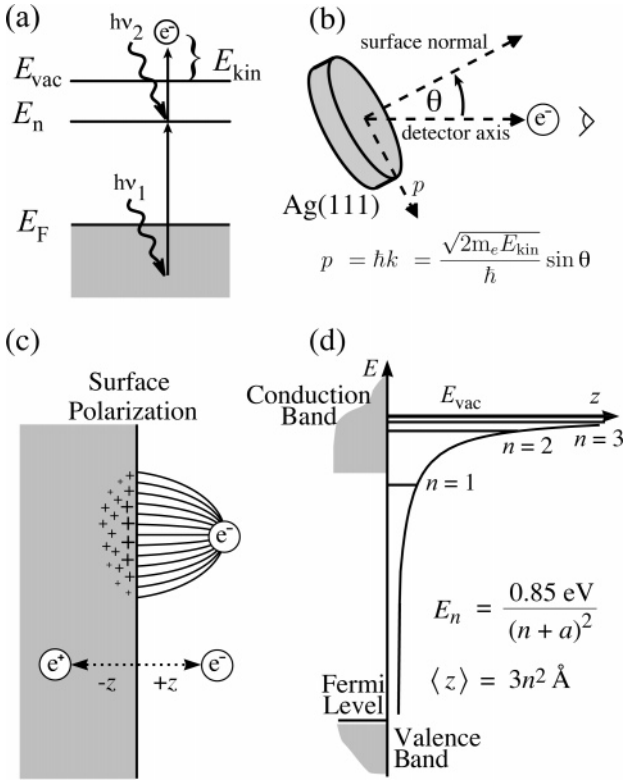

Figure 1. 2PPE of image potential states. (a) A UV photon (pump) excites an electron from the occupied states of the metal to an initially unoccupied electronic state at the surface. After a delay time, τ, a visible photon (probe) photoemits the electron sending it to a detector; (b) in angle-resolved 2PPE, only electrons with a particular amount of momentum parallel to the surface reach the detector; (c) an excess electron above a metal surface induces a surface charge which can be represented by the image of the electron reflected across the surface with the opposite charge; (d) the attraction between the electron and the image charge is a Coulomb interaction which leads to an infinite series of states with principle quantum number, n, and quantum defect parameter, a, which give binding energies E_n that converge to the vacuum level, E_{vac}.

* Corresponding author: cbharris@berkeley.edu.
† Current address: Department of Chemistry, Brookhaven National Lab, Upton, NY 11973, United States.

10.1021/jp051977z CCC: $30.25
Published on Web 09/30/2005

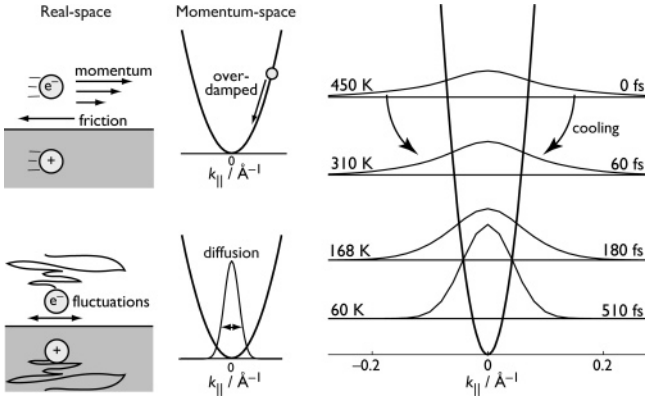

Figure 2. Friction in real space slows the IPS charge causing it to cascade down the IPS band in momentum-space. Fluctuations in the electrostatic potential will cause the charge to diffuse (random walk); in momentum-space, these impulses lead to a distribution of occupied momentum states. In the experiment, the initially photoexcited electron distribution loses energy and momentum in the IPS band and "cools" near the band minimum. The average energy is then $\langle E \rangle / k_B = T/2$, for a one-dimensional slice of the two-dimensional distribution.

with a cascading process in the IPS band, whereby electrons lose energy and momentum in successive scattering events (Figure 2).

The lifetimes of electrons as a function of their parallel momentum have been studied quantitatively in a variety of systems, such as monatomic adlayers of Xe,[5] compound interfaces such as N_2/Xe/Cu(111),[6] alkane-covered surfaces[3], and bare metal surfaces (e.g., Cu(100),[7,8] Cu(119),[9] and Ag-(100)[10]). The phonon spectra, electronic structures, and crystal structures of these systems are very different, and yet, the intraband relaxation is qualitatively similar. The momentum dependence of the IPS lifetimes has been explained in terms of phonon scattering,[5,6] electron−hole pair creation,[7] or electron localization via small polaron formation.[3] Additionally, these data have been analyzed with a phenomenological energy/momentum loss function,[6] electron transfer theory,[3] or a many-body electron scattering theory in the GW approximation.[7,8] But, the question remains: What is the simplest physical picture which can tie together the remarkably similar observations of momentum loss in these radically dissimilar systems? Here, we argue that the answer is *friction*, and that this simple concept can explain complications of previous analyses as direct consequences of the fluctuation−dissipation theorem.

The course of this argument will take us from the new experimental results of films of *p*-xylene/Ag(111) to a demonstration of how to extract a friction coefficient from 2PPE data, to comparisons to other work, and finally, to a discussion of the mechanism of the observed friction.

2. Experimental Section

The experimental apparatus has been described previously.[11] The laser system is a commercial regeneratively amplified Ti:sapphire laser which generates 250 fs pulses at 250 kHz. These drive an optical parametric amplifier (OPA), which gives tunability from 780−480 nm. A prism pair compresses the pulse to ∼120 fs autocorrelation. The OPA output is used to generate second harmonic in a type II β-barium borate (BBO) crystal. The visible fundamental (probe) and the UV second-harmonic (pump) pulses are separated. The visible pulse travels down a variable delay line after which the pulses are recombined and sent to the ultrahigh-vacuum chamber. Photoelectrons are detected by multichannel plates, and their time-of-flight is measured by time-correlated single-electron counting.

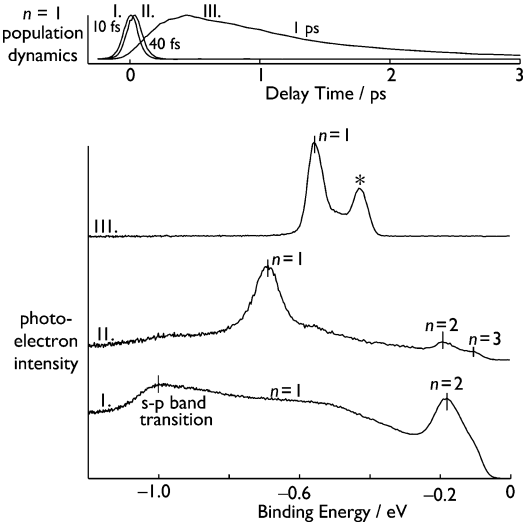

Figure 3. 2PPE of 1−3 monolayers of *p*-xylene/Ag(111) (660 nm probe wavelength) showing layer-by-layer growth. The one monolayer spectrum (I) is broad, because of poor ordering of the interface and/or hybridizing of the image state with the electron affinity of the *p*-xylene molecule. The second (II) and third (III) monolayers, however, give sharp $n = 1$ features. The population dynamics of the $n = 1$ IPS electrons at $k_{||} = 0$ give lifetimes of 10 ± 10, 40 ± 10, and 1000 ± 200 fs for one, two, and three monolayers, indicating that the IPS electrons are pushed to the film−vacuum interface as the film gets thicker.

We grow films of organic solvents such as the *p*-xylene by backfilling the main chamber with the vapor above the liquid, controlled by a variable leak valve. The solvent is degassed by multiple freeze−pump−thaw cycles, and the vapor is tested for water impurites with a quadrupole mass spectrometer. Anhydrous *p*-xylene was used as obtained from Sigma-Aldrich. Exposing the Ag(111) crystal to a pressure of 2×10^{-7} Torr (uncorrected) of *p*-xylene for 40 s (8 langmuir) corresponds roughly to a monolayer exposure. The one monolayer film was grown at 170 K and the thicker films at 115 K. All film thicknesses were determined by the evolution of the 2PPE spectra with sequential exposures of $\sim 1/4$ monolayer.

3. 2PPE of *p*-Xylene/Ag(111)

Monolayers of *p*-xylene adsorb molecularly on Ag(111) and grow in a layer-by-layer fashion (Figure 3). A coverage of one monolayer (I) gives broad 2PPE features that can be identified as $n = 1$ and $n = 2$ IPS. The breadth (0.5 eV full width at half-maximum (fwhm)) of the $n = 1$ state in the monolayer can be ascribed to poor ordering of the first *p*-xylene layer and/or hybridization of the IPS with the electron affinity level of the *p*-xylene molecule, as previously observed in naphthalene/Ag(111).[12] The peak at −1 eV binding energy is the direct sp-band transition of the substrate.[13] The second monolayer (II), however, gives sharp $n = 1$ and $n = 2$ features. Their spacing gives a quantum defect parameter $a = 0.107$ (Figure 1d) and a work function shift of −0.74 eV. Further exposure at 115 K grows a third monolayer (III) The feature marked with an asterisk is either a fourth monolayer or a different morphology with a different work function; however, we found no experimental procedure to obtain the three-monolayer coverage without this other structure, though the relative amplitudes varied as a function of annealing time and adsorption temperature. This could indicate Stranski−Krastanov growth, with a "wetting layer" that is two monolayers thick before the onset of simultaneous multilayer growth. This analysis will concentrate

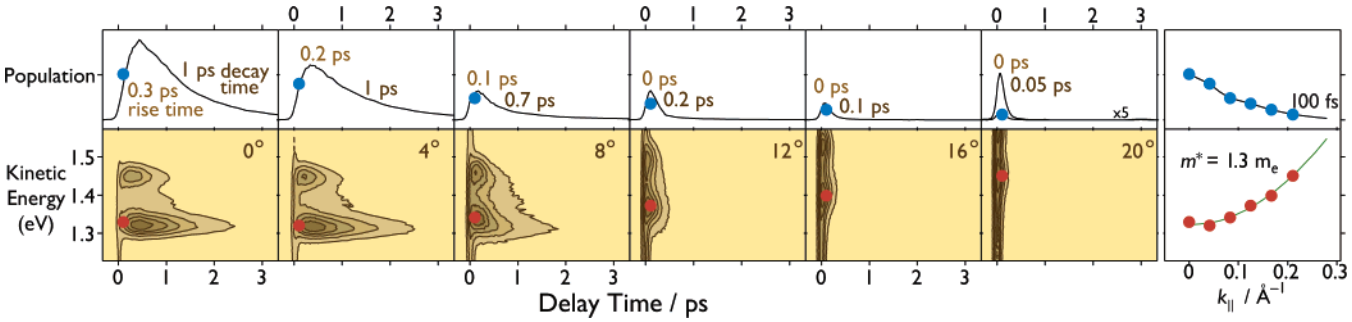

Figure 4. Angle-resolved 2PPE of two monolayers of *p*-xylene/Ag(111) from 0° to 20° (0 to ~0.2 Å^{-1}), in approximately 0.04 Å^{-1} increments. The contour plots show the evolution of the $n = 1$ IPS state as a function of delay time and angle of observation. The lower right panel summmarizes the dispersion of the energy versus parallel wavevector ($k_{||}$). Above the contour plots are fits to the population dynamics which give exponential rise and decay times. The upper right panel summarizes the population distribution vs $k_{||}$ at 100 fs delay time.

on the $n = 1$ IPS state of the third monolayer and will neglect the very similar dynamics of the feature marked ∗.

The dynamics of the $n = 1$ IPS electrons are very different in one-, two-, and three-monolayer-thick films (Figure 3). A phenomenological kinetics formula[14]

$$P(t) = A\frac{r_1}{r_1 - r_2}[\exp(-r_2 t) - \exp(-r_1 t)] \qquad (1)$$

where the $P(t)$ is the population in terms of rise and decay rates, r_1 and r_2, and A is an amplitude coefficient, describes the data well when convoluted with the laser cross-correlation function (typically a 120 fs fwhm Gaussian). The function given by Hotzel et al.[6] gives very similar results. The $n = 1$ IPS lifetimes are: 10 ± 10 fs in one monolayer, 40 ± 10 fs in two monolayers, and 1.0 ± 0.2 ps in the three monolayers. The observed decay at $p_{||} = \hbar k_{||} = 0$ is a result of the electron scattering back to the metal substrate (interband scattering).[4,8] Evidently, the third monolayer film forms a tunneling barrier that pushes the electron wave function to the layer−vacuum interface, which reduces the overlap of the IPS wave function with the substrate, thereby increasing the residence time at the surface.

The lifetimes of the $n = 1$ IPS are highly dependent on the angle of observation, that is, on the electron's momentum parallel to the surface (Figure 4). The IPS electrons's energy increases with the square of the parallel momentum, giving an effective mass $m^* = 1.3 \pm 0.1\ m_e$. For three monolayers of *p*-xylene, the lifetime at $k_{||} = 0$ is 1.0 ± 0.2 ps but drops to 0.06 ± 0.1 ps by 0.2 Å^{-1}—nearly a 20-fold decrease. As others have noted,[5,6] another important feature is that the population at zero parallel momentum *increases* as a function of the delay time. The best fit to the data gives a rise time of 0.3 ± 0.1 ps at $k_{||} = 0$ Å^{-1}, and this rise time decreases with $k_{||}$ (Figure 4). Momentum-dependent rise and decay rates such as this are clear indications of intraband relaxation.[5,6]

The error bars represent 95% confidence intervals. Some errors are surprisingly large (e.g., 1.0 ± 0.2 ps) considering the experimental pump−probe cross-correlation (120 fs). The principle cause is that eq 1 does not have the proper shape to describe the kinetics trace in detail.

Another way to see the dynamics is to examine the angular distribution of photoelectrons as a function of time. Figure 5 shows the photoelectron intensity as a function of parallel momentum at three time delays $\tau = 0$, 100, and 500 fs. Two features should be noted: first, when the amplitude is normalized to unity at $k_{||} = 0$ (Figure 5 inset), the distribution is constant from 0 to 100 fs but it narrows between 100 and 500 fs; second, the area under the unnormalized curves is clearly not conserved

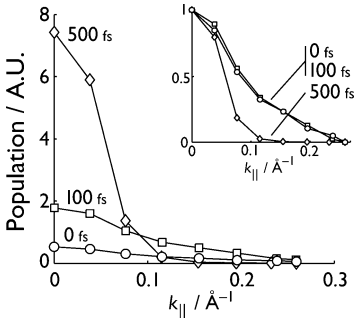

Figure 5. Population vs momentum for two monolayers of *p*-xylene/Ag(111) at three delay times, 0, 100, and 500 fs. The area under this curve is not conserved because *k*-space is two-dimensional; the two-dimensional volume-weighted area, however, is conserved. (inset) Intensity vs momentum normalized to unity at $k_{||} = 0$. This shows the narrowing of the electron distribution as a function of delay time.

as a function of the time delay—0, 100, and 500 fs have relative areas of 1:3:7. Both behaviors are depicted in Figure 2.

How can the signal increase by a factor of 7 nearly 400 fs after the pump pulse arrived at the sample? The number of electrons at the surface must be constant or decreasing because of a finite surface lifetime, so it must be the electron distribution that is changing. The 2PPE measurement only gives a slice through the two-dimensional *k*-space distribution along one axis, say k_x, and not an integrated measure of all electrons at momentum $|k_{||}|$. Therefore, the area under the experimentally measured distribution is not expected to be unity. The area under the curves weighted by the appropriate two-dimensional volume element ($2\pi \int k_{||}\, dk_{||}$), however, should be constant. The time delays of 0, 100, and 500 fs, when including the proper dimensionality, give normalized ratios of 1:3:2.6. The increase between 0 and 100 fs is a finite laser pulse duration effect, and the small decay from 100 to 500 fs is consistent with a ~1 ps decay rate tunneling back to the metal.

4. Intraband Relaxation as Friction

In this section, we will describe a method based on Smoluchowski's equation for overdamped harmonic motion—in which the friction is a parameter—that simulates the momentum-resolved 2PPE data numerically.

In the simplest approximation, a friction force, F_x, is linear in the electron's velocity, $\dot{x}$

$$F_x = -\Gamma_x \dot{x} \qquad (4.1)$$

where Γ_x is the coefficient of friction in *x*-space. In stochastic models of dynamics (e.g., Brownian motion), the particle of interest is coupled to a bath. In this case, the IPS electron is

coupled to the bath of electrons and phonons of the substrate and adlayer (section 5). The resulting random forces lead to both a diffusive random walk and also a linear friction. Thus, the diffusion coefficient, D_x, is related to the friction (and temperature) directly via

$$D_x = k_B T/\Gamma_x \tag{4.2}$$

where k_B is Boltzmann's constant and T is the temperature.

Perhaps surprisingly, the dynamics of these free electrons in k-space are isomorphic with the dynamics of an overdamped harmonic oscillator (Figure 2). The electron's kinetic energy, $\hat{T} = \hat{P}^2/2m^*$, acts as the potential energy of the harmonic oscillator, and friction is a "restoring force" that brings the electron to the bottom of the IPS band. The relationship between the friction in x-space and k-space, however, must be established. The presence of friction in x-space, Γ_x, pulls the electron to the bottom of the band of k-states. The larger the friction, Γ_x, the faster the electron falls to the bottom of the band. Conversely, if the electron were perfectly free, $\Gamma_x = 0$, then the electron would stay in its initial k-state indefinitely. This physical picture shows that the frictions in real and momentum-space must be inversly proportional; simple considerations show this to be exactly so (Appendix I)

$$\Gamma_x = 1/\Gamma_{p_x} = \hbar^2/\Gamma_{k_x} \tag{4.3}$$

where Γ_{p_x} is the friction in momentum-space, and Γ_{k_x} is the friction in k-space ($\mathbf{p} = \hbar\mathbf{k}$).

Fundamentally, the dynamics of a harmonic oscillator depend on both a generalized coordinate and its conjugate momentum, but in the high-friction (Smoluchowski) limit, the motion is overdamped and only the generalized coordinate remains in the dynamical equations of motion. Being overdamped specifically means that the generalized momentum is fully equilibrated at every instant and, thus, carries no dynamical information. All the information resides in the generalized coordinate and the friction kernel. Assuming that the motion of the electron in k-space is overdamped allows us to map the momentum-space dynamics of a free electron onto an overdamped harmonic oscillator.

This assumed high friction limit *in momentum-space* is appropriate, because the electrons are very free in configuration-space. The electrons drift to a thermally equilibrated distribution at the bottom of the IPS band and stay there. Underdamped motion in k-space cannot occur for free electron—oscillations happen when the total energy moves between potential energy and kinetic energy— but these free particles have only kinetic energy, so no oscillations are possible. This point emphasizes that the electrons are not harmonic oscillators, but the same mathematics for overdamped harmonic motion describes the dynamics of these free particles in k-space. As an aside, note that the equilibrium is between a single IPS electron and the bath (meaning all modes of the system to which the electron is coupled), not between many IPS electrons. The relevant temperature is not a true electronic temperature but, rather, the temperature of the substrate.

The dynamics of a distribution of overdamped harmonic oscillators have an analytical solution if the friction is Markovian.[15,16] The distribution, p, given at any initial time, t_0, can be propagated forward, exactly, to any other time, t, by the appropriate Green function, G. That is, letting k_x represent the generalized coordinate

$$p(k_x, t|k_{x0}, t_0) = \int_{-\infty}^{\infty} dk_{x0}\, G(k_x, t|k_{x0}, t_0)\, p(k_{x0}, t_0) \tag{4.4}$$

where the Green function is

$$G(k_x, t|k_{x0}, t_0) = \left(\frac{1}{2\pi\sigma_{k_x}^2(t)}\right)^{1/2} \exp\left(-\frac{[k_x - \langle k_x\rangle(t)]^2}{2\pi\sigma_{k_x}^2(t)}\right) \tag{4.5}$$

Equation 4.5 has the structure of a normalized Gaussian with a time-dependent average position, $\langle k_x\rangle(t)$, and width, $\sigma_{k_x}(t)$. These correspond to drift and diffusion, respectively, and can be expressed as

$$\sigma_{k_x}^2(t) = \frac{D_{k_x}(1 - e^{-2B_{k_x}(t-t_0)})}{B_{k_x}} \tag{4.6a}$$

$$\langle k_x\rangle(t) = k_{x0}\, e^{-B_{k_x}(t-t_0)} \tag{4.6b}$$

The propagator, G, carries the influence of the friction coefficient, Γ_{k_x}, through the variables D_{k_x} and B_{k_x}. The variable D_{k_x} represents diffusion of the electrons in k-space, and so, it depends on both the temperature and the friction

$$D_{k_x} = k_B T/\Gamma_{k_x} \tag{4.7}$$

The variable, B_{k_x}, on the other hand, gives the characteristic rate of motion in the IPS band, so it depends on the curvature of the band, $\partial^2\hat{H}/\partial k_x^2$, which for the case of the nearly free IPS electrons is $\hbar^2/m^*$. So

$$B_{k_x} = \frac{\hbar^2}{m^*\Gamma_{k_x}} \tag{4.8}$$

Already, the theory has the structure we desire—the drift term (eq 4.6b) pulls the electrons to the bottom of the IPS band, and diffusion (eq 4.6a) leads to a Boltzmann distribution of electrons equilibrated to the sample temperature.

These formulas have been generalized to two dimensions,[16] as is appropriate because $k_{||}$ has x and y components. The relevant formulas become

$$p(k_x, k_y, t|k_{x0}, k_{y0}, t_0) = \int\int_{-\infty}^{\infty} dk_{x0}\, dk_{y0}\, G(k_x, k_y, t|k_{x0}, k_{y0}, t_0) p(k_{x0}, k_{y0}, t_0) \tag{4.9}$$

$$G(k_x, k_y, t|k_{x0}, k_{y0}, t_0) = \left(\frac{1}{2\pi\sigma_{k_x}(t)\sigma_{k_y}(t)}\right) \exp\left(-\frac{1}{2}Q(t)\right) \tag{4.10}$$

$$Q(t) = \left(\frac{k_x - \langle k_x\rangle(t)}{\sigma_{k_x}}\right)^2 + \left(\frac{k_y - \langle k_y\rangle(t)}{\sigma_{k_y}}\right)^2 \tag{4.11}$$

and

$$\sigma_{k_x}^2(t) = \frac{D_{k_xk_x}(1 - \exp(-2B_{k_xk_x}(t - t_0)))}{B_{k_xk_x}} \quad (4.12a)$$

$$\langle k_x\rangle(t) = k_{x0}\exp(-B_{k_xk_x}(t - t_0)) \quad (4.12b)$$

$$\sigma_{k_y}^2(t) = \frac{D_{k_yk_y}(1 - \exp(-2B_{k_yk_y}(t - t_0)))}{B_{k_yk_y}} \quad (4.12c)$$

$$\langle k_y\rangle(t) = k_{x0}\exp(-B_{k_yk_y}(t - t_0)) \quad (4.12d)$$

Here, D_{ii} and B_{ii} are derived from the diagonal components of the friction tensor Γ_{ij}.[16] If the friction tensor is symmetric, i.e., the friction is the same for k_x and k_y, then we can use only one index to label $\Gamma_{k_xk_x} \equiv \Gamma_{k_yk_y} \equiv \Gamma_k$. This assumption holds for (111) surfaces but will certainly fail for stepped surfaces.[9,17,18]

Because the dynamics of the electron distribution are analytical for all future times, simulations can use eq 4.9 as a zeroth-order propagator and then include population relaxation dynamics as a correction term in a grid-based approach[15,16]

$$p(k_x, k_y, t|k_{x0}, k_{y0}, t_0) = \int\int_{-\infty}^{\infty} \mathrm{d}k_{x0}\,\mathrm{d}k_{y0}$$
$$G(k_x, k_y, t|k_{x0}, k_{y0}, t_0)p(k_{x0}, k_{y0}, t_0) - \kappa_0 p(k_{x0}, k_{y0}, t_0)\Delta t \quad (4.13)$$

where κ_0 is the rate of tunneling back to the metal. This scheme allows reasonably large step sizes to be taken (in this work, 10−30 fs). Typical k-space grids span −0.5 to 0.5 Å^{-1}, with a grid spacing of ∼0.01 Å^{-1}.

Careful work has shown that the tunneling rate does change with $k_{||}$ because of the band structure of the substrate.[4,7] As the IPS energy gets closer to the conduction band edge, the wave function overlap in the metal increases, which increases the rate of tunneling from the IPS back to the metal. These effects are typically estimated by calculating the IPS wave function using a simple dielectric continuum model (DCM). Unfortunately, the DCM does not correctly give wave functions or lifetimes of IPS electrons, because the electron affinity (EA) of *p*-xylene is positive. In the calculation, this draws the wave function into the layer, near the surface, making the lifetime too short. More sophisticated calculations that include the molecular details explicitly[19−21] and account for both the electron-attractive aromatic moiety and the electron-repulsive alkyl moieties of the *p*-xylene might produce better agreement with the data. Nevertheless, even when the dependence of the lifetime on momentum can be calculated correctly, the effect does not dominate the observed dynamics,[5,6] as long as the electrons do not cross above the conduction band edge. Therefore, we will approximate the relaxation rate κ_0 as constant with $k_{||}$ in this work; future work may correct this simplification.

In this way, the initial distribution excited to the surface as determined by the experiment (Figure 5) can be used as a starting configuration for the simulation. Also measured in the experiment are the curvature of the IPS band, given by the effective mass, m^*, and the population relaxation rate, κ_0, determined at the bottom of the IPS band, $r_2(k_{||} = 0)$. More carefully, $\kappa_0 = r_2(k_{||} = 0)$ is true only if there is a reasonable separation of inter- and intraband relaxation time scales $\kappa_0 \ll B_{k_x}$, which holds for these experiments. Otherwise, the decay constant that describes the experimental kinetics, r_2, will overestimate the true population decay time. Of the variables in the theory (eqs 4.7 and 4.8), then, only the friction coefficient, Γ_k, is a free parameter. The value of Γ_k, the friction in k-space, is determined by matching the simulations to the experimental kinetics.

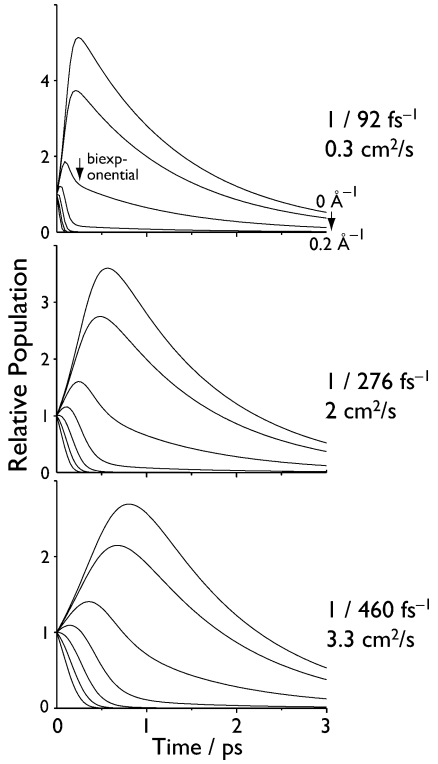

Figure 6. Simulated dynamics using the two-dimensional Smoluchowski equation for three different rates of motion, $B = {}^1/_{92}$, ${}^1/_{276}$, and ${}^1/_{460}$ fs^{-1}. The curves represent the population at different $k_{||}$ from 0 to 0.2 Å^{-1} in 0.04 Å^{-1} steps. In all three cases, the tunneling rate $\kappa_0 = {}^1/_{1.2}$ ps^{-1}. The population at low parallel momentum increases for several hundred femtoseconds. The decay rate increases with increasing parallel momentum. Biexponential decays show the crossover from intraband relaxation to population decay (interband relaxation) after the distribution has approached the Boltzmann distribution at the bottom of the band.

The initial distribution is based on peak intensities from the data, which are scaled up by $1/\cos^4\theta$, where θ is the angle between the surface normal and the laser polarization, to account for screening of the parallel component of the electric field by the metal. The initial intensity distribution (Figure 5) was parametrized by two gaussians centered at $k_{||} = 0$ of fwhm 0.12 and 0.31 Å^{-1} and relative amplitudes 0.9:1, respectively.

The spirit of these calculations is very similar to the work of Hotzel et al.,[6] but their phenomenological energy and momentum loss function has been replaced with a propagator that is a general consequence of a particle being coupled to a bath under the assumptions that (1) the motion of the IPS electrons in k-space is overdamped, (2) the friction is linear in the generalized velocity, and (3) that the friction is Markovian (no memory). By construction, this propagator obeys the fluctuation−dissipation theorem, and it has only one degree of freedom not directly constrained by experiment, namely, the friction coefficient. In fact, a substantial difference in interpretation with Hotzel et al.[6] rests on the lack of fluctuations (diffusion) in that model (section 5).

Typical simulated dynamics show all of the features expected from the experiment (Figure 6). Presented are simulations with lifetime $\kappa_0 = {}^1/_{1200}$ fs^{-1} and with three different k-space friction coefficients (diffusion constants), namely, 500, 1500, and 2500 eV Å^2 fs, (0.67, 2, and 3.3 cm^2/s). The rates of motion in k-space, B_{k_x}, for the three cases are ${}^1/_{92}$, ${}^1/_{276}$, and ${}^1/_{460}$ fs^{-1}. The temperature is $T = 100$ K, which corresponds to a Boltzmann distribution fwhm of 0.094 Å^{-1} (standard deviation 0.040) Å^{-1}.

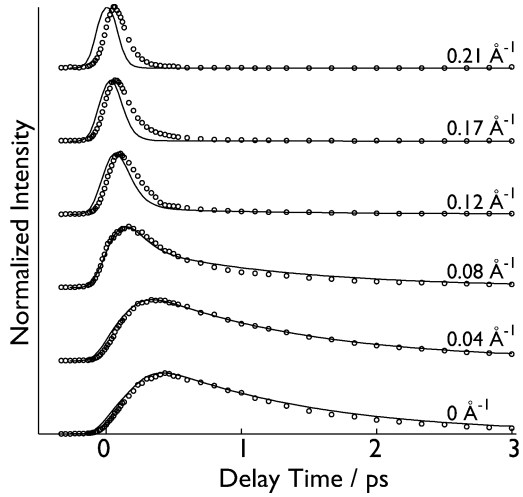

Figure 7. Comparison of kinetics calculated with the 2D Smoluchowski equation and the experimental data for two monolayers of *p*-xylene/Ag(111).

In all cases, the population at $k_{||} = 0$ increases for several hundred femtoseconds (usually for a time $\sim 2/B_{k_x}$), then decays with the rate $\kappa_0 \approx {}^1/_{1000}$ fs^{-1}. The momentum relaxation manifests itself as a filling of the *k*-state. After 2−3 times $1/B_{k_x}$, however, only tunneling back to the metal occurs. At high parallel momenta ($k_{||} > 0.12$ Å^{-1}), the rise time is short (or zero), and the decay rate is much faster. At these high angles, the electrons rapidly move to lower momenta, and the decay time primarily reflects the rate of intraband relaxation.

Intermediate momenta, for example, 0.08 Å^{-1} in Figure 6, show biexponential behavior. The signal has a quick rise and decay within ∼400 fs, but then switches to a longer time scale population decay that is nearly equivalent to the $k_{||} = 0$ relaxation rate. During the first, rapid time scale, the electron distribution is still "cooling". As the electron distribution approaches the Boltzmann distribution, however, the relaxation time scale switches to the slower rate of tunneling back to the metal. At intermediate momenta, near the half-width of the thermal distribution (∼0.05 Å^{-1}), both intra- and interband relaxation appear in the kinetics. At high momenta, only the fast momentum relaxation rate appears, because these momenta are only vanishingly present in the Boltzmann distribution.

Note that the momentum distributions in Figure 6 do not continue to relax to delta functions at $k_{||} = 0$, because this stochastic model of friction includes fluctuations as well as dissipation. As the distribution reaches the bottom of the IPS band, fluctuations, i.e., diffusion in momentum space, compete with the dissipation. The Boltzmann distribution gives the equilibrium between these two forces, obeying detailed balance.

The friction coefficient can be determined by the best fit of the simulations to the experimental kinetics (Figure 7). To account for the finite angular acceptance of the detector, which effectively weights the measurement to higher momenta,[10,22] the simulation is averaged over the appropriate region of *k*-space. The best-fit friction coefficient is $\Gamma_k = 1200 \pm 500$ eV Å^2 fs or, equivalently, using eq 4, $\Gamma_x = 6 \times 10^{-18}$ kg/s. The effective diffusion constant is $D_x = 2$ cm^2/s at the experimental temperature of 100 K. Simulations show biexponential behavior near 0.08 Å with the correct time constants. The agreement between the simulation and the data, however, is not perfect. At the highest angles, the simulated signal does not rise for the same length of time as the experimental kinetics, likely because the highest momenta (0.22 Å) are near the edge of the simulation grid (0.25 Å) and not enough population exists in the simulation to continue to fill the high-momenta states. Also, we cannot measure the electron distribution past ∼0.27 Å^{-1}, leaving the distribution there uncertain. We have approximated it as a gaussian; if the real distribution is wider, it will also lead to extra signal appearing at high angles, as will transfer from higher IPS states into $n = 1$.[9] Nevertheless, the agreement between simulations and experiment supports the idea that intraband relaxation can successfully be described as friction.

5. Discussion

So far, we have developed a method to simulate 2PPE data, but let us examine some analytical consequences of representing intraband relaxation as overdamped motion in the IPS band. Consider the limit in which the rate of decay back to the substrate is greater than the rate of motion in *k*-space, i.e., $\kappa_0 > B_{k_x}$. This should be a reasonable assumption for both clean metal surfaces[7,10] and noble-gas monolayers,[5,19,20,23,24] as the maximum in 2PPE signal at $k_{||} = 0$ is near $t = 0$. That is, the electrons decay back to the metal before they have time to slow appreciably. For any particular momentum, there are two relaxation channels for the electrons: tunneling back to the substrate and scattering to a lower momentum. Let us approximate the former, for this argument's sake, to be independent of $k_{||}$ as discussed previously. The latter is equivalent to a velocity (pointing to $k_{||} = 0$) in momentum space and is related to the Green function, eq 4.10. This can be evaluated by taking the instantaneous velocity in momentum space, v_k, (the time derivative of the average position given by eq 4.12b) evaluated at $t = t_0$

$$v_k = \frac{\mathrm{d}}{\mathrm{d}t}\langle k_x(t)\rangle|_{t=t_0} = \frac{\mathrm{d}}{\mathrm{d}t}(k_x - k_{x0}\,\mathrm{e}^{-B_{k_x}(t-t_0)})|_{t=t_0}$$
$$= B_{k_x} k_{x0} \tag{5.1}$$

Thus, this simple picture of overdamped motion on a parabolic surface predicts that the rate of transfer to lower momenta should scale linearly with the initial parallel momentum, and the first derivative of the velocity in *k*-space versus $k_{||}$ is B_{k_x}.

Indeed, at least one recent 2PPE study of intraband relaxation (Wong et al.) has shown a linear increase of intraband relaxation rate as a function of $k_{||}$. Wong et al. studied intraband relaxation in Xe/Ag(111). They converted the momentum dependent decay constants to an effective line width, *L*, which is directly proportional to the rate of decay, r_2 in eq 3.1

$$\frac{L}{\hbar} = r_2(k_{||}) = 1/\tau_\mathrm{d}(k_{||}) \tag{5.2}$$

where $\tau_\mathrm{d}(k_{||})$ is the decay time as a function of the parallel wavevector. They separated the inter- and intraband components of the decay rate (denoted ⊥ and ||, respectively) and set the interband component to be independent of $k_{||}$

$$r_2(k_{||}) = r_{2||}(k_{||}) + r_{2\perp} \tag{5.3}$$

Because no intraband relaxation is possible at $k_{||} = 0$, the decay rate at the band minimum only reflects interband relaxation

$$r_2(k_{||} = 0) = r_{2\perp} \tag{5.4}$$

Thus

$$r_{2||}(k_{||}) = r_2(k_{||}) - r_2(k_{||} = 0) \tag{5.5}$$

When plotted, $r_{2||}$ appears to be a linear function of $k_{||}$.

Additionally, the slope of this line decreases as the Xe film thickness increases.

We can go past such a simple parametrization of the dynamics and look at more subtle consequences of including fluctuations in the dynamics. Equation 5.1 shows that the rate of decay increases linearly with parallel momentum, but when electrons are long-lived and can equilibrate to the sample temperature, fluctuations cause even more structure in the observed rise and decay times. These time constants can change rapidly as a function of momentum, depending on which momenta are appreciably populated at equilibrium. The half-width or standard deviation of the Boltzmann distribution is a reasonable indicator of this transition region. For many experiments in the literature, this is $\sim$0.04 Å^{-1}. Below $\sim$0.04 Å^{-1}, the signal rises as the electron distribution cools and decays slowly as the electrons tunnel back to the metal. Above this range, however, there is no rise time, and the rate of decay increases rapidly because intraband relaxation is an available decay pathway. In the transition region, more complex biexponential dynamics occur. Behavior of this variety has been observed in, for example, *n*-heptane/Ag(111)[3] and N_2/Xe/Cu(111),[6] but this richness in dynamical behavior needs no explaination more complicated than friction.

Omitting the fluctuations can lead to some spurious results. One system in which the angle-resolved 2PPE kinetics of intraband relaxation was explicitly modeled was the compound interface of N_2/Xe/Cu(111).[6] The results of those experiments are very similar to what we see in *p*-xylene/Ag(111). The lifetimes of the $n = 1$ IPS are several picseconds, and the 2PPE intensity at $k_{||} = 0$ increases for a full 1 picosecond because of electrons cascading down the IPS band. Hotzel et al. modeled these dynamics using a phenomenological energy-loss function to accurately fit the photoemission rise and decay. Most notably, however, their energy-loss function included a lower bound, an energy below which the loss of energy could no longer occur. Their estimate of this bound was 6 ± 4 meV, which they ascribed to a quantized librational mode of the N_2 overlayer. To show that this electron−phonon scattering mechanism was reasonable, they calculated the scattering cross-section of the quasi-two-dimensional IPS electron with a free N_2, which gave reasonable agreement to the observed intraband relaxation.

We propose, however, that the low-energy cutoff in this model is an artifact, because the kinetic equations include energy loss but not energy fluctuations. In practice, Hotzel et al.[6] introduced the smallest energy that could be lost because the data decay too slowly at small, but finite, parallel momentum, (0.07 Å^{-1}, for example). Without a low-energy cutoff, the energy-loss function that they propose predicts that all electrons should relax to $k_{||} = 0$. In other words, theirs is a zero temperature ($T = 0$) theory. Because the temperature is nonzero, however, there must be excitations which impart momentum back to the electrons, exciting them back up into the band. We believe that their measurements are entirely correct. There is a change in the observed time scales of relaxation—most visible in Figure 3 of Hotzel et al.[6] Rather than a quantized loss of energy, however, the change in dynamics is probably due to the electron distribution approaching its thermal equilibrium value. To see that this is reasonable, note that the temperature of the experiments is 20 K, or 2 meV, which, though not identical, is very similar to the low-energy cutoff required in their model.

So far, this discussion has concentrated on electrons which are delocalized parallel to the interface, but some systems cause the IPS electrons to localize. Accurately modeling the electron localization in these two-dimensional systems is of interest to theory, because the two-dimensional case is the so-called "marginal case", where the driving forces for localization and delocalization are nearly balanced. Experimental examples where localization occurs include two or more monolayers of *n*-heptane/Ag(111),[3] nitriles/Ag(111),[2] and D_2O/Cu(111).[1] The case of *n*-heptane/Ag(111) was specifically interpreted in terms of small polaron formation through a theory that maps polaron formation to Marcus electron transfer theory. In this formalism, the kinetic energy of the electron is the largest contribution to the free energy of localization (ΔG), so electrons of different momenta should localize at different rates. The rate of decay of photoemission signal at different momenta was attributed to electron localization only; Ge et al.[3] acknowledged the importance of intraband decay pathways but did not model them explicitly.

We can extend our work to include the dynamics of localization by making an analogy to barrierless chemical reactions.[15] In this picture, the delocalized IPS states are intermediates which can react (i.e., localize) to form products (i.e., localized electrons) with a rate depending on a reaction coordinate ($k_{||}$). We rewrite eq 4 to include a sink term, $S(k_x, k_y)$, which is a function of k_x and k_y and explicitly sets the relative rates of localization as a function of the momentum in the plane

$$p(k_x, k_y, t|k_{x0}, k_{y0}, t_0) = \int\int_{-\infty}^{\infty} \mathrm{d}k_{x0}\, \mathrm{d}k_{y0} G(k_x, k_y, t|k_{x0}, k_{y0}, t_0) p(k_{x0}, k_{y0}, t_0) - \kappa_0\, p(k_{x0}, k_{y0}, t_0)\Delta t - \kappa_l S(k_{x0}, k_{y0}) p(k_{x0}, k_{y0}, t_0)\Delta t \quad (5.6)$$

where κ_l is the overall rate of localization. This formulation does not supply a hypothesis for the form of $S(k_x, k_y)$ but will allow a proposed mechanism to be tested. Indeed, the theory that was applied to *n*-heptane/Ag(111)[3] makes very specific predictions of how the rate of localization should change as a function of the momentum of the electron. These predictions can generate a sink function *S*, and with eq 5.6, one can simulate electron localization simultaneous with intraband relaxation to refine our mechanistic understanding of electron localization in two dimensions.

For the case of Brownian motion of a dust mote, the mechanism of system−bath coupling is obvious—the collisions with gas atoms and molecules. The IPS electron, on the other hand, is in a vacuum at the surface of an atomically flat substrate, so where do the random forces come from? There are three sources of electron scattering: electron−electron, electron−phonon, and electron−defect interactions.[8] The electrons and phonons of the subtrate and adlayer are at nonzero temperature, so they can both accept energy from and impart energy to the electron in a stochastic fashion. Defect scattering, on the other hand, is not properly described by a stochastic picture. For the case of IPS electrons, electron−electron interactions[7,8] prove sufficient to reproduce the experimental friction coefficient.

The most sophisticated analysis of inter- and intraband relaxation of IPS electrons at metal interfaces uses the GW approximation to the electron self-energy to calculate the scattering mediated by the substrate electrons.[7,8,25] This allows one to solve, approximately, the quantum-mechanical many-body scattering problem by calculating matrix elements of the imaginary part of the screened Coulomb interaction operator, Im*W*. The low-energy part of the excitation spectrum, calculated quantum mechanically, fixes the intraband decay rate, and the method correctly includes the detailed nature of the initial and final states of the decay process. This analysis quite elegantly

shows that because the overlap between states within the IPS band is greater than the IPS and the substrate, the rates of inter- and intraband scattering can be comparable for clean metal surfaces though the driving forces are very different.[7] This method provides the most complete and accurate derivation of the friction experienced by a charge. Nevertheless, it remains difficult to extend these calculations to interfaces of molecular adsorbates.

Within the framework of this many-body electron scattering theory, however, some simplifying assumptions make the calculation of a friction coefficient tractable: (1) The electron is a point charge moving parallel to the metal surface at a fixed distance, z, and (2) the response of the metal can be described by the specular reflection model and the Lindhard dielectric function in the random phase approximation. This latter approximation treats the valence electrons of the substrate as a free-electron gas perfectly contained by the surface. The Lindhard dielectric function includes damping due to both one-electron excitations (electron−hole pairs due to interband transitions) as well as collective excitations (plasmons). The friction due to these two interactions scales differently with z (collective response like z^{-3} and one-electron scattering like z^{-4}), so, far enough from the surface, the collective response will always dominate the observed friction.

Undamped plasmon states cannot be excited by low-energy electrons, but when damping is included, electrons of arbitrarily small energy above the Fermi level can give energy to the plasmon field.[26] The asymptotic limit ($z \gg v/\omega_s$, where v is the velocity of the electron and ω_s is the surface plasmon frequency) of the friction due to damped plasmons, $\Gamma_{1,x}$, is[26,27]

$$\Gamma_{1,x} = \frac{(Ze)^2}{4\pi\epsilon_0}\frac{\gamma}{4\omega_p^2 z^3} \tag{5.7}$$

where $\omega_p = \sqrt{2}\omega_s$ is the bulk plasmon frequency, γ is the damping of the plasmons, Z is the total charge of the particle of interest, and ϵ_0 is the permittivity of free space. This result is equivalent to the friction an image charge would experience because of the finite conductivity of the substrate[28−31]

$$\Gamma_{1,x} = \frac{1}{4\pi\epsilon_0}\frac{(Ze)^2}{16\pi\sigma z^3} \tag{5.8}$$

which can be derived by classical electrodynamics[28−30] or statistical mechanics.[31] Here, σ is the dc conductivity of the substrate material in gaussian units of reciprocal seconds, where $9 \times 10^{11}\ s^{-1} = 1\ (\Omega\ cm)^{-1}$, and z is the distance from the particle to the surface. Estimating the distance above the surface as $z = 3$ Å, $\sigma = 2.4 \times 10^6\ (\Omega\ cm)^{-1}$,[32] and $T = 100$ K, we find $\Gamma_{1,x} = 1 \times 10^{-19}$ kg/s. This is much less than the experimentally determined friction constant in *p*-xylene/Ag(111).

The asymptotic limit of the friction due to interband one-electron excitations is[26,27]

$$\Gamma_{2,x} = \frac{m(Ze)^2}{4\pi\epsilon_0}\frac{24}{\pi}\frac{\ln(k_{TF}z/1.4475)}{(2k_{TF}z)^4} \tag{5.9}$$

where k_{TF} is the Thomas-Fermi screening wavevector. For surface parameters ($r_s = 2.97\ a_0$,[33] where $a_0 = 0.53 \times 10^{-10}$ m is the Bohr radius, and $k_{TF} = 2.95\ Å^{-1}(r_s/a_0)^{-1/2} = 1.71\ Å^{-1}$)[34] gives $\Gamma_{2,x} = 3.3 \times 10^{-17}$ kg/s at a distance $z = 3$ Å. This is much larger than $\Gamma_{1,x}$ and shows the dominance of this mechanism at these length scales.

The asymptotic limit is not appropriate at a few angstroms, however. Numerical integration of eq 29−30 of Núñez et al.[27] gives refined values of the friction $\Gamma_{1,x} = 2.8 \times 10^{-18}$ kg/s when the plasmon damping is $\hbar\gamma = 0.4$ eV, and $\Gamma_{2,x} = 1.9 \times 10^{-17}$ kg/s, for a total $\Gamma_{tot,x} = \Gamma_{1,x} + \Gamma_{2,x} = 2.18 \times 10^{-17}$ kg/s. At $z = 5$ Å, this drops to $\Gamma_{tot,x} = 4.9 \times 10^{-18}$ kg/s. Because of the simplicity of the model, one should not expect quantitative agreement with the experimental result, but this range brackets the experimentally measured friction coefficient, 6×10^{-18} kg/s, and indicates that electron−electron scattering with the substrate electrons is sufficent to explain the observed dynamics. Because the friction should have the same order of magnitude for all the noble metals, electron−electron scattering may also have been the dominant dissipative interaction in the N_2/Xe/Cu(111) experiments of Hotzel et al.[6] rather than scattering off the N_2 phonons.

So, the following picture emerges. Because the IPS electron is so close to the surface of the metal substrate, the substrate valence electrons cannot effectively screen it. Subsequent electron−electron collisions cause electron−hole pair excitations (interband transistions). Finally, electron−hole pairs can be thermally excited and give their energy and momentum back to the IPS electron. Damped surface plasmons provide a secondary, minor channel for energy dissipation.

Several research groups have started to look at the role that controlled defects, in the form of stepped metal surfaces, have in the mechanism of intraband relaxation.[9,17,18,35] They have observed that the dynamics differ if the electron momentum is directed along a terrace or across the steps. The dynamics may even be anisotropic depending on whether the electron travels "upstairs" or "downstairs".[17] The methods developed here could be extended to these systems using a friction tensor with different eigenvalues to describe motion in the different momentum directions. Simulations of this kind could describe both the rise and decay times of the IPS electrons in these measurements. The electronic structure of the substrate can be quite different in the different k-space directions in these systems, so one should carefully test the validity of simplistic assumptions such as the interband lifetime being independent of $k_{||}$. The efficiency of steps at promoting population transfer among the IPS of different principle quantum number, however, would complicate the analysis.

Our understanding of the variety of electron decay pathways at metal interfaces has made a great deal of progress in recent years.[8] The simple physical picture developed here may help one to analyze 2PPE data in a manner that is physically meaningful and theoretically tractable in systems more complex than clean metal surfaces and noble-gas monolayers. Under the assumptions that (1) the motion of the IPS electrons in k-space is overdamped, (2) the friction is linear in the generalized velocity, and (3) the friction is Markovian (no memory), we can model the time- and angle-resolved 2PPE data. This analysis gives a friction coefficient that is reasonably matched by the theory of electron−electron scattering,[8,26,27] with one-electron excitations as the dominating contribution to energy dissipation. As 2PPE is applied to more complex interfaces, this is likely to be an active area of research, relevant not only to the 2PPE community but also to all those interested in the friction due to dielectric fluctuations.[31,36] The 2PPE measurements may be ideal testbeds for these theoretical developments because of the controlled probe (an electron whose charge does not fluctuate), single-crystal substrates, and (when the surface science permits) variable film thicknesses of different dielectric materials.

Acknowledgment. We would like to thank K. J. Gaffney, C. M. Wong, and J. D. Jackson for stimulating discussions and an anonymous reviewer for suggesting the use of the Lindhard dielectric function. Supported by the director, Office of Energy Research, Office of Basic Energy Sciences, Chemical Sciences Division for the U.S. Department of Energy, under contract DE-AC03-76SF00098. We acknowledge NSF support for specialized equipment used in these experiments.

Appendix I. Momentum Friction vs Real Space Friction

Ignore all random, fluctuating forces for a moment (equivalent to setting $T \rightarrow 0$) and consider only a single particle's trajectory with initial velocity $\dot{x} = \dot{x}_0$. The frictional force will lead to a change in momentum

$$F_x = \frac{\mathrm{d}p}{\mathrm{d}t} \tag{I.1}$$

Using the definition of a friction linear in the velocity, eq 4.1, and the dynamics in momentum-space (analogous to eq 4.6b), we see

$$-\Gamma_x \dot{x} = \frac{\mathrm{d}}{\mathrm{d}t}\left[p_{x0} \exp(-B_{p_x} t)\right] \tag{I.2}$$

$$= -B_{p_x} p(t) \tag{I.3}$$

Here, p represents the momentum of a particle, not the distribution of particles in k-space, $p(k, t)$. Of course, $p(t) = \dot{x}(t)$, and with the definition of $B_{p_x} = 1/m^*\Gamma_{p_x}$, we have

$$\Gamma_x = \frac{1}{\Gamma_{p_x}} \tag{I.4}$$

The friction in k-space can be related to the friction in p-space by unit analysis considering the generalized forces, $F_{p_x} = -\partial H/\partial p_x$ and $F_{k_x} = -\partial H/\partial k_x$, where H is the Hamiltonian of the free particle, or directly to Γ_x by a procedure similar to eq I.2, giving

$$\Gamma_x = \frac{\hbar^2}{\Gamma_{k_x}} \tag{I.5}$$

References and Notes

(1) Gahl, C.; Bovensiepen, U.; Frischkorn, C.; Wolf, M. *Phys. Rev. Lett.* **2002**, *89*, 107402.
(2) Miller, A. D.; Bezel, I.; Gaffney, K. J.; Garrett-Roe, S.; Liu, S. H.; Szymanski, P.; Harris, C. B. *Science* **2002**, *297*, 1163−1166.
(3) Ge, N.-H.; Wong, C. M.; Lingle, R. L., Jr.; McNeill, J. D.; Gaffney, K. J.; Harris, C. B. *Science* **1998**, *279*, 202−205.
(4) Fauster, T.; Steinmann, W. In *Electromagnetic Waves: Recent Devlopments in Research: Photonic Probes of Surfaces*; Halevi, P., Ed.; Elsevier: Amsterdam, 1995; Vol. 2, Chapter 8, p 349.
(5) Wong, C. M.; McNeill, J. D.; Gaffney, K. J.; Ge, N.-H.; Miller, A. D.; Liu, S. H.; Harris, C. B. *J. Phys. Chem. B* **1999**, *103*, 282−292.
(6) Hotzel, A.; Wolf, M.; Gauyacq, J. P. *J. Phys. Chem. B* **2000**, *104*, 8438−8455.
(7) Berthold, W.; Höfer, U.; Feulner, P.; Chulkov, E. V.; Silkin, V. M.; Echenique, P. M. *Phys. Rev. Lett.* **2002**, *88*, 056805.
(8) Echenique, P. M.; Berndt, R.; Chulkov, E. V.; Fauster, T. H.; Goldmann, A.; Höfer, U. *Surf. Sci. Rep.* **2004**, *52*, 219−317.
(9) Weinelt, M. *J. Phys.: Condens. Matter* **2002**, *14*, R1099−R1141.
(10) Giannetti, C.; Galimberti, G.; Pagliara, S.; Ferrini, G.; Banfi, F.; Fausti, D.; Parmigiani, F. *Surf. Sci.* **2004**, *566*, 502−507.
(11) Lingle, R. L., Jr.; Ge, N.-H.; Jordan, R. E.; McNeill, J. D.; Harris, C. B. *Chem. Phys.* **1996**, *205*, 191−203.
(12) Gaffney, K. J.; Miller, A. D.; Liu, S. H.; Harris, C. B. *J. Phys. Chem. B* **2001**, *105*, 9031−9039.
(13) Miller, T.; McMahon, W. E.; Chiang, T. C. *Phys. Rev. Lett.* **1996**, *77*, 1167−1170.
(14) Steinfeld, J. I.; Francisco, J. S.; Hase, W. L. *Chemical Kinetics*, 2nd ed.; Prentice Hall: London, 1998.
(15) Bagchi, B.; Fleming, G. R. *J. Phys. Chem.* **1990**, *94*, 9−20.
(16) Poornimadevi, C. S.; Bagchi, B. *Chem. Phys. Lett* **1990**, *168*, 276−282.
(17) Roth, M.; Pickel, M. T.; Wang, J. X.; Weinelt, M.; Fauster, T. *Phys. Rev. Lett.* **2002**, *88*, 096802.
(18) Shen, X.; Kwak, H.; Radojevic, A.; Smadici, S.; Mocuta, D.; Osgood, R. *Chem. Phys. Lett.* **2002**, *351*, 1−8.
(19) Berthold, W.; Rebentrost, F.; Feulner, P.; Höfer, U. *Appl. Phys. A* **2003**, *78*, 131−140.
(20) Marinica, D. C.; Ramseyer, C.; Borisov, A. G.; Teillet-Billy, D.; Gauyacq, J. P.; Berthold, W.; Feulner, P.; Höfer, U. *Phys. Rev. Lett.* **2002**, *89*, 046802.
(21) Marinica, D. C.; Ramseyer, C.; Borisov, A. G.; Teillet-Billy, D.; Gauyacq, J. P. *Surf. Sci.* **2003**, *540*, 457−473.
(22) Bezel, I.; Gaffney, K. J.; Garrett-Roe, S.; Liu, S. H.; Miller, A. D.; Szymanski, P.; Harris, C. B. *J. Chem. Phys.* **2004**, *120* (2), 845−856.
(23) Berthold, W.; Feulner, P.; Höfer, U. *Chem. Phys. Lett.* **2002**, *358*, 502−508.
(24) Berthold, W.; Höfer, U.; Feulner, P.; Menzel, D. *Chem. Phys.* **2000**, *251*, 123−132.
(25) Kliewer, J.; Berndt, R.; Chulkov, E. V.; Silkin, V. M.; Echenique, P. M.; Crampin, S. *Science* **2000**, *288*, 1399−1402.
(26) Ferrell, T. L.; Echenique, P. M.; Ritchie, R. H. *Solid State Commun.* **1979**, *32*, 419−422.
(27) Núñez, R.; Echenique, P. M.; Ritchie, R. H. *J. Phys. C: Solid State Phys.* **1980**, *13*, 4229−4246.
(28) Shier, J. S. *Am. J. Phys.* **1968**, *36*, 245−249.
(29) Boyer, T. H. *Am. J. Phys.* **1999**, *67*, 954−958.
(30) Schaich, W. L. *Phys. Rev. E* **2001**, *64*, 046605.
(31) Tomassone, M. S.; Widom, A. *Phys. Rev. B* **1997**, *56*, 4938−4943.
(32) Lide, D. R., Ed. *Handbook of Chemistry and Physics*, 85th ed.; CRC Press: Boca Raton, FL, 2004.
(33) Bastidas, C. L.; Liebsch, A.; Mochían, W. L. *Phys. Rev. B* **2001**, *63*, 165407.
(34) Ashcroft, N. W.; Mermin, N. D. *Solid State Physics*; Thomas Learning: Toronto, 1976.
(35) Fauster, T. *Surf. Sci.* **2002**, *507*, 256−263.
(36) Zurita-Sánchez, J. R.; Greffet, J.-J.; Novotny, L. *Phys. Rev. A* **2004**, *69*, 022902.